Water-Window Soft X-Ray Spectra from Dual Laser-Produced Bi Plasmas*)

Tomoyoshi TOIDA[1)], Tsukasa SUGIURA[1)], Hayato YAZAWA[1)], Hiroki MORITA[1)], Shinichi NAMBA[2)] and Takeshi HIGASHIGUCHI[1)]

[1)]*Department of Electrical and Electronic Engineering, Utsunomiya University, Utsunomiya 321-8585, Japan*
[2)]*Department of Advanced Science and Engineering, Hiroshima University, Higashihiroshima 739-8527, Japan*

(Received 15 July 2024 / Accepted 10 September 2024)

We described the spectral behavior of the water-window soft x-ray emission in detail by dual laser pulse irradiation. We also observed the spatial separation of the soft x-ray emission and fast ions produced using dual pulse irradiation. Soft x-ray emission distribution was almost isotropic, and the fast ions were emitted to the target normal along the pre-pulse laser axis. The soft x-ray emission was maximized at a delay time of 50 ns between the pre-pulse, and the main laser heating pulse when the pre-plasma was irradiated at a distance of 50 μm above the target.

Keywords: water window, soft x-ray, optical thickness, bismuth, highly charged ion (HCI)

DOI: 10.1585/pfr.20.2406003

1. Introduction

Soft x-ray (SXR) emission, ranging from the oxygen K-edge (O_K-edge) at 2.3 nm to the carbon K-edge (C_K-edge) at 4.4 nm, so-called the water-window (WW), is of significant interest due to its importance for high-resolution *in vivo* microscopic imaging of biological structure in samples such as cells and macromolecules. Low-debris table-top, efficient SXR sources have been demonstrated by gas jets [1] and double-stream gas puff targets [2]. On the other hand, the emission power and conversion efficiency are high due to the presence of unresolved transition arrays (UTAs) in their spectra from a higher atomic number element plasmas, which consist of many resonant lines due to the overlapping of 4p - 4d and 4d - 4f ($\Delta n = 0$) resonance transitions around specific wavelengths, as compared to the lower atomic number element plasma. The peak wavelengths of the UTA emission obey a "quasi-Moseley's law" [3, 4]. In the WW-SXR spectral region, the candidate element is bismuth (Bi) [5, 6], plasmas of which provide intense UTA emission around 4 nm that can be coupled to a high-reflectivity coefficient multilayer mirror [7].

In the laser-ablations and laser-produced plasmas, the direction of the radiation and the debris, including the fast ions and the neutral particles, whose spatial distribution followed a cosine function, were generally the same [8, 9]. The collector mirror for radiation sets the position angles of the target normal in the semiconductor lithography and the close angle of the target normal in the microscope system. The collector mirror is exposed to debris particles. Its lifetime is expected to be shorter. In the SXR microscope, one of the solutions is the use of the grazing incidence mirror [7]. However, the mirror is coated by laser ablation debris for a longer operation. Therefore, the focus is on the feasibility of spatially separating the EUV emission and debris generation. One of the solutions that reinforces this possibility is found in the cross-laser-injection configuration for solid-target-based soft x-ray lasers (SXL) and for high-order harmonic generation (HHG) [10, 11]. The emission direction of the debris, which includes the fast ions, clusters, and fragments, is normal to the target for pre-plasma production through the laser ablation. The pump laser (main laser) is incident along the tangential direction to the target surface. On the other hand, we expect the isotropic distribution of the SXR emission from a point-like-hot, dense plasma. There is no data on the spatial distribution separation and the SXR spectral behavior under the cross-laser-injection configurations for the WW-SXR microscope.

In this paper, we focus on the spatial distribution separation of the SXR emission and the fast ions under the cross-laser-injection configurations. The SXR emission spectral behavior is also observed by changing the delay time between the pre- and main pulses.

2. Experimental Condition

Figure 1 shows a schematic diagram of the experimental apparatus. Two *Q*-switched Nd:yttrium-aluminum-garnet (Nd:YAG) lasers operating at a wavelength of 1064 nm for the pre-pulse and main heating pulse were employed. The two laser systems were synchronized using a pulse delay oscillator (Stanford Research Systems Inc.,

author's e-mail: higashi@cc.utsunomiya-u.ac.jp

*) This article is based on the presentation at the 26th International Conference on Spectral Line Shapes (ICSLS2024).

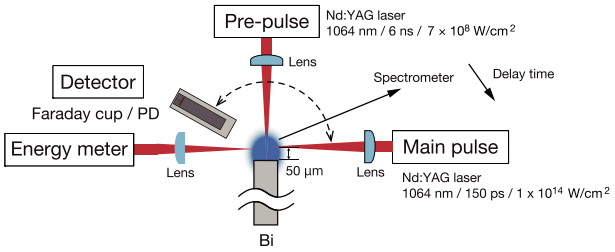

Fig. 1 Schematic diagram of the experimental apparatus.

DG645) with a jitter of less than 1 ns. The fluctuations in pulse energy were approximately 2% in both laser systems. The pre-plasma was generated on the edge of a planar Bi target with a thickness of 1 mm.

The intensity of the 6-ns pre-pulse was 7×10^8 W/cm^2 at a pulse energy of 210 mJ and a focal spot diameter of 2.5 mm. The beam was loosely focused to produce a large volume of pre-ionized plasma (pre-plasma). The pre-pulse irradiated the target at normal incidence and 90° to the main laser axis. The main laser irradiated the pre-plasma at a distance of 50 μm above the target surface at a delay time of D_t = 10 - 150 ns after the pre-pulse laser. Note that time delay of 50 ns was found to be optimal value to measure the SXR emission angular distribution with sufficient photon flux. The main laser intensity was kept at 1×10^{14} W/cm^2, at a pulse energy of 110 mJ with a pulse duration of 150 ps and a focal spot diameter of 30 μm.

Using a rotated Faraday cup (FC) as an ion collector, we measured the angular distribution of Bi ions from the plasma. The angular distribution of Bi ions in different charge states should be useful in optimizing the placement of the collector mirror. We observed the spectra using a flat-field grazing incidence spectrometer with an unequally ruled 2400 grooves/mm grating. The spectrometer was positioned at 30° with respect to the incident main laser axis. Time-integrated SXR spectra were recorded by a thermo-electrically cooled back-illuminated x-ray charge-coupled device (CCD) camera (Andor Technology Inc.). The typical spectral resolution was better than 0.01 nm. The spectrometer has been absolutely calibrated [12]. The pressure inside the vacuum chamber was kept at 1×10^{-4} Pa.

3. Experimental Results and Discussion

The angular distribution of the fast Bi ions plays an important role in determining where the sensitive collector mirror should be located. Figure 2 shows the angular distributions of the SXR emission and the ion charge of fast ions, with the pre-pulse, at a delay time of 50 ns measured by a rotated SXR diode with a 500-nm thin-Ti foil filter to cut the infrared (IR), visible, and ultraviolet (UV) emission in front of the x-ray detector in the spectral region of 2.8 - 7 nm and the FC to detect the fast ions.

The target was located at the origin of Fig. 2. The pre-

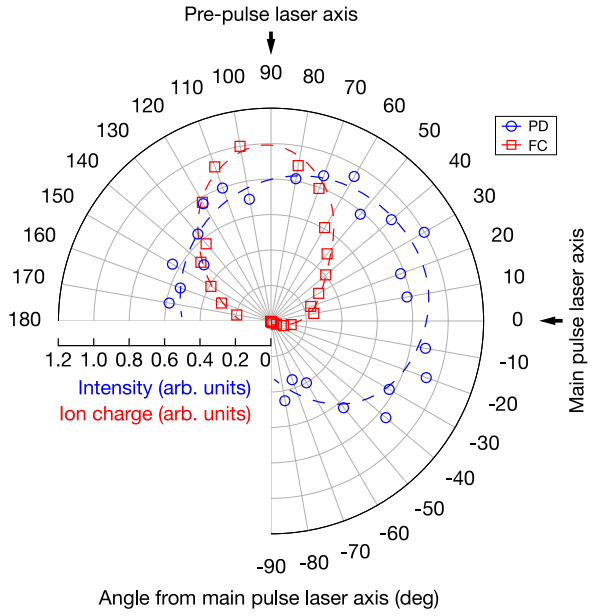

Fig. 2 Angular distributions of the SXR emission by the photodiode (PD) and fast ion charge by the Faraday cup (FC).

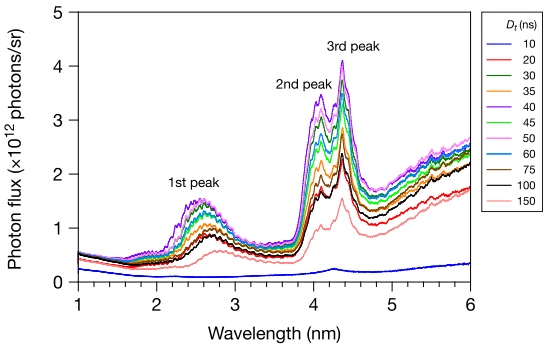

Fig. 3 Time-integrated SXR spectra at different delay times of D_t ranging from 10 to 150 ns.

pulse propagated along the 90° direction. The SXR emission has a quasi-isotropic distribution. It is seen that the angular distribution of the fast ions has a sharp peak in the direction normal to the target. The angular distributions are fitted with a $\cos^n\theta$-function, and good agreement is obtained with $n \approx 3$.

Figure 3 shows the time-integrated SXR spectra at different delay times of D_t ranging from 10 to 150 ns. The optimum delay time between the pre-pulse and the main laser pulse was 50 ns at 50 μm from the target surface. The unresolved transition array (UTA) spectra were attributed to the $n = 4 - n = 4$ transition in the wavelength region of 4 - 4.2 nm and the $n = 4 - n = 5$ transitions in the wavelength region of 1.6 - 3.6 nm. We discuss the opacity in the plasmas related to the emissivity and absorption processes using the observed spectra [6].

Time-integrated SXR spectra between 1 and 6 nm display strong broadband emission near 4 nm, which mainly

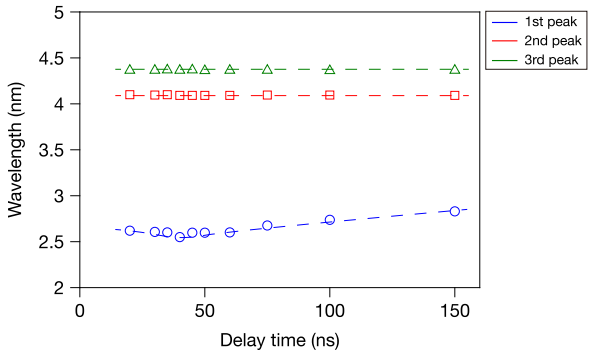

Fig. 4 Peak wavelengths of three peaks at different delay times of D_t ranging from 10 to 150 ns.

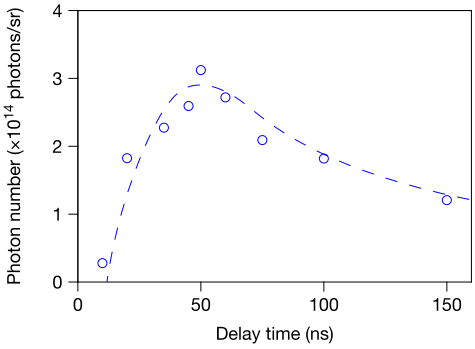

Fig. 5 WW-SXR photon number as a function of the delay time from Fig. 3.

originates from $n = 4 - n = 4$ transitions from ions with an open 4f or 4d outermost subshell, together with broadband emission around 1.6 - 3.6 nm originated from $n = 4 - n = 5$ transitions from multi-charged state ions with an outermost 4f subshell. The intensity of the $n = 4 - n = 4$ UTA emission is higher than that of the $n = 4 - n = 5$ emission [13]. Note that the vertical axis corresponds to the number of photons within a bandwidth of 0.01 nm in Fig. 3. The self-absorption by the Bi plasma is low because the effective electron temperatures of the maximized emissivity and opacity were different [6]. In the present scheme in Fig. 1, we produced the optically thin Bi plasma, and the SXR absorption effect is low.

Figure 4 shows the peak wavelength change of three emission intensity peaks in Fig. 3 as a function of the delay time. The peak wavelength of the $n = 4 - n = 4$ transition emission is observed to be unchanged. On the other hand, the peak wavelength of the $n = 4 - n = 5$ transition emission is shifted to a shorter wavelength by increasing the emission intensity of the $n = 4 - n = 4$ transition emission toward the delay time of D_t = 30 - 50 ns because of the rise in the electron temperature and associated charge states.

The WW-SXR photon number as a function of the delay time from Fig. 3 is shown in Fig. 5. The maximum number of photons is maximized at the delay time of 50 ns. We also observed the main pulse transmission along the main laser axis by the energy meter in Fig. 1. The transmission coefficient was minimized at the same pulse delay of 50 ns. This means that the laser absorption of the main laser pulse energy is maximized, resulting in the emission maximized, as shown in Figs. 3 and 5. For further understanding of the laser absorption process, we should conduct the radiation hydrodynamic simulation [14].

4. Summary

In summary, we have described the spectral behavior of the water-window SXR emission by dual laser pulse irradiation. We have achieved the feasibility of spatial separation of the SXR and the fast ion emission under the cross-laser-injection configurations. Spatial distributions of the SXR emission and the fast ion were almost isotropic and a $\cos^3\theta$ distribution, respectively. The fast ion was emitted to the target normal along the pre-pulse laser axis. The SXR emission was maximized at a delay time of 50 ns between the pre-pulse and the main laser heating pulse under the pre-plasma was irradiated at a distance of 50 μm.

Acknowledgments

The authors are indebted to Masaki Kume and Takeru Niinuma (Utsunomiya University) for practical technical support and discussion. T.H. acknowledges the support from the Japan Society for the Promotion of Science (JSPS) / INTERNATIONAL JOINT RESEARCH PROGRAM and The Sumitomo Foundation.

[1] M. Müller *et al.*, Opt. Express **21**, 12831 (2013).
[2] P.W. Wachulak *et al.*, Appl. Phys. B **118**, 573 (2015).
[3] H. Ohashi *et al.*, Appl. Phys. Lett. **104**, 234107 (2014).
[4] Y. Shimada *et al.*, AIP Adv. **9**, 115315 (2019).
[5] T. Higashiguchi *et al.*, Appl. Phys. Lett. **100**, 014103 (2012).
[6] G. Arai *et al.*, Opt. Express **26**, 27748 (2018).
[7] T. Hatano *et al.*, J. Electron Spectrosc. Relat. Phenom. **220**, 14 (2017).
[8] T. Higashiguchi *et al.*, Rev. Sci. Instrum. **76**, 126102 (2005).
[9] T. Higashiguchi *et al.*, Appl. Phys. Lett. **88**, 161502 (2006).
[10] Y. Nagata *et al.*, Phys. Rev. Lett. **71**, 3774 (1993).
[11] D. von der Linde *et al.*, Phys. Rev. A **52**, R25(R) (1995).
[12] T.-H. Dinh *et al.*, Rev. Sci. Instrum. **87**, 123106 (2016).
[13] T. Wu *et al.*, J. Phys. B **49**, 035001 (2016).
[14] A. Sunahara *et al.*, Opt. Express **31**, 31780 (2023); and references therein.